

Three-dimensional transient temperature field model for laser annealing

Jean-Yves Degorce,^{a)} Jean-Numa Gillet, François Magny, and Michel Meunier^{b)}

Department of Engineering Physics, École Polytechnique de Montréal, Laser Processing Laboratory, C.P. 6079, succ. Centre-ville, Montréal, Québec H3C 3A7, Canada

(Received 21 June 2004; accepted 12 November 2004; published online 11 January 2005)

A three-dimensional transient temperature field model (TTFM) is proposed for the general problem of laser-induced out-of-equilibrium annealing of a bilayer device, which is made up of a bulk material covered by a transparent layer. The TTFM solves the moving-boundary problem with a deterministic relation between the interface velocity and temperature in contrast to preceding problem-dependent models, which use an interface-tracking heuristic algorithm. The TTFM is the first step to model many temperature-driven phenomena such as diffusion and segregation in laser annealing. Both computed transient temperature field and melted-zone dimensions of a SiO₂/Si example device, which is irradiated by a focused visible (532 nm) laser, are in very good agreement with experimental measurements. © 2005 American Institute of Physics. [DOI: 10.1063/1.1846943]

I. INTRODUCTION

Laser interactions with materials may lead to various surface processes including melting, texturing, hardening, and ablation. At moderate fluence, the effect of a pulsed laser may be limited to surface melting, which can be used for example to redistribute dopants incorporated into a silicon device.^{1,2} For an extended nonfocused laser beam, this problem can be simplified to a one-dimensional one for which numerical and analytical solutions exist. However, focusing a pulsed laser on a target surface (as in the case of texturing a hard disk drive³ or analog-device trimming^{1,2}) requires solution of three-dimensional (3D) differential equations with boundary conditions (BC) moving with the solid–melt interface. Unfortunately, it is not possible to derive an exact analytical solution for the 3D problem of the moving solid–liquid boundary. Therefore, only approximate analytic solutions can be obtained from the heat-transfer balance equations.^{4,5} On the other hand, preceding numerical approaches to solve the problem of laser-induced melting and recrystallization,^{6,7} in which out-of-equilibrium BCs must be used instead of the usual equilibrium ones, involve interfacial response functional relationships of the solution itself. Such heuristic modeling requires a solution-dependent tracking algorithm to locate the interface position and therefore is very computationally demanding. To avoid this problem, we propose in this paper an out-of-equilibrium transient temperature field model (TTFM), which uses a deterministic relationship between the interface velocity and temperature.⁸ Our model allows one to compute the interface position and transient temperature field without using any further problem-dependent algorithm. To validate our approach, we first compare simulation results obtained from the out-of-equilibrium model to those from the equilibrium one, where the interface temperature is set to the equilibrium melting temperature of the material. Then, we perform experimental measurements on a bulk silicon covered by a thin (0.5 μm)

transparent SiO₂ cap, which is irradiated by a focused ($r_0 = 0.9 \mu\text{m}$) Nd:YAG laser ($\lambda = 532 \text{ nm}$), as shown in Fig. 1. Since the validity of the numerical model depends on its capability to predict the melted-zone dimensions and transient temperature field, we carry out two different experiments: First, we show the good agreement between the computed dimensions and atomic force microscopy (AFM) measurements of the melted surface. Second, from the temperature-dependent optical properties of bulk Si,^{9,10} we perform transient reflectivity measurements to evaluate the surface transient temperature field, which is successfully compared to the simulation results.

II. STATEMENT OF THE PHYSICAL PROBLEM AND MATHEMATICAL FORMULATION

Usually the transient temperature field induced by focused-laser irradiation onto an absorbing solid is not only due to heat diffusion but also to the penetration depth of the laser light, which depends on the optical absorption. Laser-induced heating changes the optical properties of the material owing to their temperature dependence. The dissipated-energy distribution can be obtained from the Maxwell equations¹¹ and finite-difference time-domain modeling. However, this problem can be considerably simplified with common assumptions.¹² The volume heat source term in the heat equation, which is due to laser–material interaction,

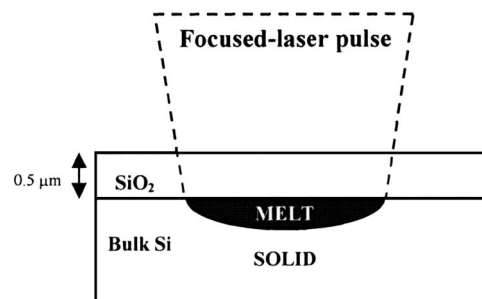


FIG. 1. Scheme of a focused visible laser that irradiates a bilayer substrate made up of a thin transparent layer (SiO₂) and a bulk absorbing layer (Si).

^{a)}Corresponding author: Electronic mail: jean-yves.degorce@polymtl.ca

^{b)}Corresponding author: Electronic mail: michel.meunier@polymtl.ca

clearly depends on both optical absorption α and reflectivity R for the wavelength λ and temperature T under consideration. The α and R variations with T also make the source term dependent on T . This dependence is essential at the phase-change temperature because the optical properties of the material such as the optical absorption and reflectivity may exhibit dramatic variations between the solid and liquid phases. Realistic simulation of a focused-laser annealing process must therefore be carried out from 3D calculations, including all temperature dependencies of the material parameters α , ρ , c , and κ , where ρ is the mass density, c the specific heat at constant pressure, and κ the thermal conductivity. To do this, we consider the bilayer problem of an absorbing solid (bulk Si) covered by a transparent cap (SiO_2), as show in Fig. 1. The cap prevents the convection movement at the liquid surface since no significant distortion of the material surface appears when a bilayer is processed by laser annealing.¹³

Owing to the use of a Gaussian laser beam, problem modeling is axis-symmetric and includes (i) optical absorption; (ii) heat diffusion in both materials with a phase change in the absorbing material; and (iii) reflectivity of a probing laser. All parameters are taken to be temperature dependent. Our original mathematical formulation enables us to consider the same equations for either solid or melted absorbing material. This is different from the preceding heuristic models,^{6,7} where the material is divided into two subdomains when melting is taking place: (i) the solid and (ii) the melt, with different thermal properties. A difficulty arises in this approach because the interface between the solid and melt moves with time, so that solution-dependent BCs have to be defined at the interface, which is very computationally demanding. We avoid this problem since, with our new formulation, we obtain a unique equation which can be applied through the entire domain with no special reference to either the solid or melt. Indeed, because the only independent parameter is the temperature field $T(r, z, t)$, where r , z , and t are the respective radial, depth, and time coordinates, the other material parameters can be easily computed from simple step functions of T with transitions at the defined interface temperature.

The temperature distribution induced by laser-radiation absorption within the substrate can be calculated by using the classical heat equation given by

$$\rho(T)c(T)\frac{\partial T}{\partial t} = \nabla[\kappa(T)\nabla T] + Q(T) + L(T), \quad (1)$$

where $L(T)$ is the material's latent melting heat. While the source term Q is zero in the transparent layer, in the absorbing solids, $Q(R, \alpha, I, t)$ depends on both material and laser parameters. This term is exhaustively described in Ref. 12. The laser intensity $I(r, z)$ is solution of the Lambert-Beer equation

$$\partial I(r, z)/\partial z = \alpha(T, \lambda)I(r, z). \quad (2)$$

Equations (1) and (2) constitute the classical model formulation of the heating and melting problem. However, as explained before, we define all material parameters independently of the phase by using step functions at the interface

temperature, which enables us to avoid solution-dependent BCs.

The sudden release of energy induced by the phase change at the interface temperature is obtained from the classical enthalpy model¹⁴ as

$$\Delta H(T) = \int_{T_\infty}^T \rho(T)c(T)dT + U(T - T_{\text{int}})L(T_{\text{int}}), \quad (3)$$

where $\Delta H(T)$ keeps track of the total enthalpy accumulated at any point in the material.

In Eq. (3), T_∞ is the temperature far from the processed area, and $U(T - T_{\text{int}})$ is a Heaviside function at the interface temperature T_{int} , which is zero if $T < T_{\text{int}}$ and unity if $T > T_{\text{int}}$. Then, from the time derivation $\partial \Delta H / \partial t = \partial \Delta H(T) / \partial T \times \partial T / \partial t$, we introduce an apparent heat capacity formulation

$$\rho(T)c_{\text{app}}(T) = \rho(T)c(T) + \delta(T - T_{\text{int}})\rho(T)L(T_{\text{int}}), \quad (4)$$

where $c_{\text{app}}(T)$ is the apparent specific heat capacity. However, owing to the Dirac function $\delta(T - T_{\text{int}})$, this formulation suffers from a singularity at T_{int} . We bypass this difficulty by assuming that the phase change occurs over a small temperature interval. Therefore, we approximate the Dirac function by a Gaussian function with a characteristic width ΔT , which can be as small as a few kelvin. A second difficulty is due to the steep change of the absorbing-material thermal conductivity at the melting temperature. In order to avoid numerical instabilities, T must therefore be removed from the divergence term in Eq. (1), which can be achieved by using a Kirchhoff transform

$$\Theta(T) = \int_{T_\infty}^T \frac{\kappa(T)}{\kappa(T_\infty)} dT, \quad (5)$$

where $\Theta(T)$ is the Kirchhoff temperature of the absorbent layer and can be easily calculated by developing $\kappa(T)$ through a power series.¹²

Another Kirchhoff transform is used for the transparent-layer temperature to obtain that Θ_{TL} of Kirchhoff. In terms of Θ and Θ_{TL} , the classical equation system of Eqs. (1)–(4) transforms to

$$\frac{1}{D(\Theta)} \frac{\partial \Theta(T, t)}{\partial t} = \nabla^2 \Theta(T) + \frac{Q_p(\Theta, t)}{\kappa(T_\infty)}, \quad (6)$$

$$\frac{1}{D_{\text{TL}}(\Theta)} \frac{\partial \Theta_{\text{TL}}(T, t)}{\partial t} = \nabla^2 \Theta_{\text{TL}}(T), \quad (7)$$

in the absorbing material and in the transparent layer, respectively. In Eqs. (6) and (7), $D = \kappa / \rho c$ denotes the thermal diffusivity. The solution of this TTFM formulation can be obtained by solving simultaneously Eqs. (2), (6), and (7) in the (r, z) plane with a finite-element method (FEM). The BCs of the FEM are given in Fig. 2. For the boundary Γ , we ensure temperature continuity, i.e., $\Theta = \Theta_{\text{TL}}$, and an incident irradiation: $I = I_0 \{1 - R[T(z=0)]\} q(t) \exp[-(r/r_0)^2]$.

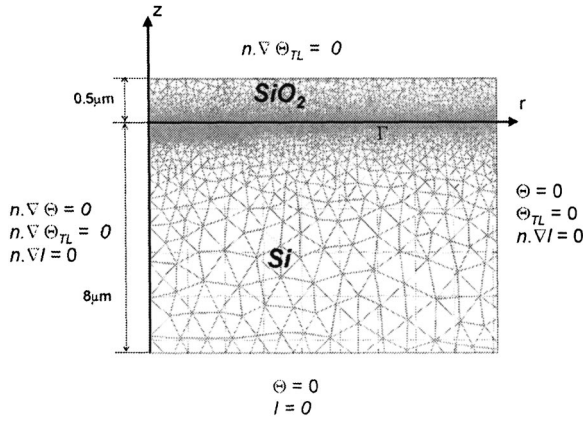


FIG. 2. Model mesh with Si and SiO₂ domains and boundaries. r and z denote the radius and depth axis. The mesh is refined within the melted zone and at the Si/SiO₂ interface. The BCs are given for the Kirchhoff temperature and laser intensity.

III. SIMULATION RESULTS FROM THE TRANSIENT TEMPERATURE FIELD MODEL

Since our model can be applied to any transparent/absorbent bilayer, we chose similar experimental conditions to those of the recently developed process of the laser-induced diffusible resistance.¹ Simulations are performed for a bulk Si covered by a thin (0.5 μm) SiO₂ layer irradiated by a 532 nm laser, which is focused with a radius of 0.9 μm and pulse width of 40 to 70 ns.

A. Equilibrium approach

In the equilibrium TTFM, the interface temperature is approximated by the equilibrium melting temperature, which is $T_{\text{eq},m} = 1683$ K for bulk Si. By performing numerical simulations, we can derive characteristic parameters of the laser process such as melting duration, and radius and depth of the melted zone as well as its dynamics. Control of the maximum temperature rise, which always occurs at the center of the laser beam ($r=0, z=0$), is important because this temperature must remain in a small temperature range between the melting points of Si (1683 K) and SiO₂ (1980 K). The transient behavior of the center point and those at $r=0.5$ and 1 μm on the Si surface, are compared in Fig. 3. The center point melts first and solidifies last because it receives the maximum amount of laser beam energy. $T(r=0, z=0)$ reaches $T_{\text{eq},m}$ within a time τ_m after the laser energy onset and, subsequently, $T(r=0, z=0)$ increases much more slowly since the absorbed laser energy is spent not only on heating but also on melting. Moreover, the steep increase of R at the melting temperature amplifies this phenomenon. The maximum in T is approximately reached at the end of the laser pulse with a duration τ_l and is followed by the silicon cooling down and resolidification within a time τ_s . From the times τ_l , τ_s , and τ_m , we can deduce the Si melting duration: $\tau_s - \tau_m$. For different times around the pulse duration, we show in Fig. 4(a) the temperature on the irradiated surface $T(r, z=0)$ and that along the z axis $T(r=0, z)$ in Fig. 4(b). From these figures, we first deduce that the maximum r and z of the melted region are first reached approximately at the end of a laser pulse (depending on the temporal pulse shape).

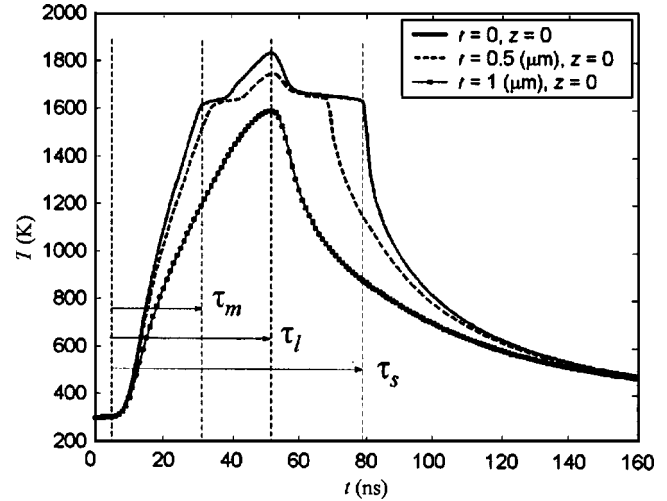


FIG. 3. Temperatures at the center point ($r=0, z=0$) and two other points on the surface irradiated by a single Gaussian laser pulse with the maximum laser intensity $I_0 = 1.35 \times 10^7$ W/cm², laser beam radius $r_0 = 0.85$ μm, and pulse duration $\tau_l = 40$ ns.

Second, this model provides at all times the values of the molten radius and depth. During laser irradiation, the surface temperature primarily depends on the beam-intensity distribution, which is characterized by the beam radius r_0 , while T along the z axis depends on heat diffusion with a typical length $l_T \approx 2\sqrt{D\tau_l}$. This difference in the heating phenomenon explains why the melt radius r_{melt} can be one order of magnitude higher than the melt depth z_{melt} .

B. Out-of-equilibrium approach

The out-of-equilibrium dynamics of interface-mediated phase transformations such as undercooling and overmelting has been the subject of considerable theoretical and experimental research.^{15,16} Since no evidence of overheating was reported in Si,⁹ only undercooling during the solidification stage has to be considered here. It is generally accepted that the deviation of the interface temperature T_{int} from $T_{\text{eq},m}$ is related to the normal velocity v_{sl} of the solid-liquid interface.^{12,16} A good assumption of the degree of undercooling in liquid Si is $T_{\text{eq},m} - T_{\text{int}} \ll T_{\text{eq},m}$, which leads to a linear form for v_{sl} ^{12,16}

$$v_{\text{sl}} = K(T_{\text{eq},m} - T_{\text{int}}), \quad (8)$$

where K is a proportionality constant. By using transient reflectivity measurements described in Sec. V, we obtained $K = 6.5$ cm s⁻¹ K⁻¹, which is comparable to the values of 6.5 to 7.5 cm s⁻¹ K⁻¹ given in previous studies.^{15,16} From Eq. (8), we note that the large radial interface velocity of the focused-laser process induces a significant deviation between T_{int} and $T_{\text{eq},m}$, in particular on the Si surface where the solidification velocity is maximal.

Efficient software to resolve the global parametric problem including absorption and heat transfer cannot be achieved with a parametric dependence of the phase-change temperature owing to the prohibitive computational cost.¹⁷ To bypass this problem, we derive a simple and accurate method based on the observation that the interface velocity is almost stable during the cooling stage. Figures 5(a) and 5(b)

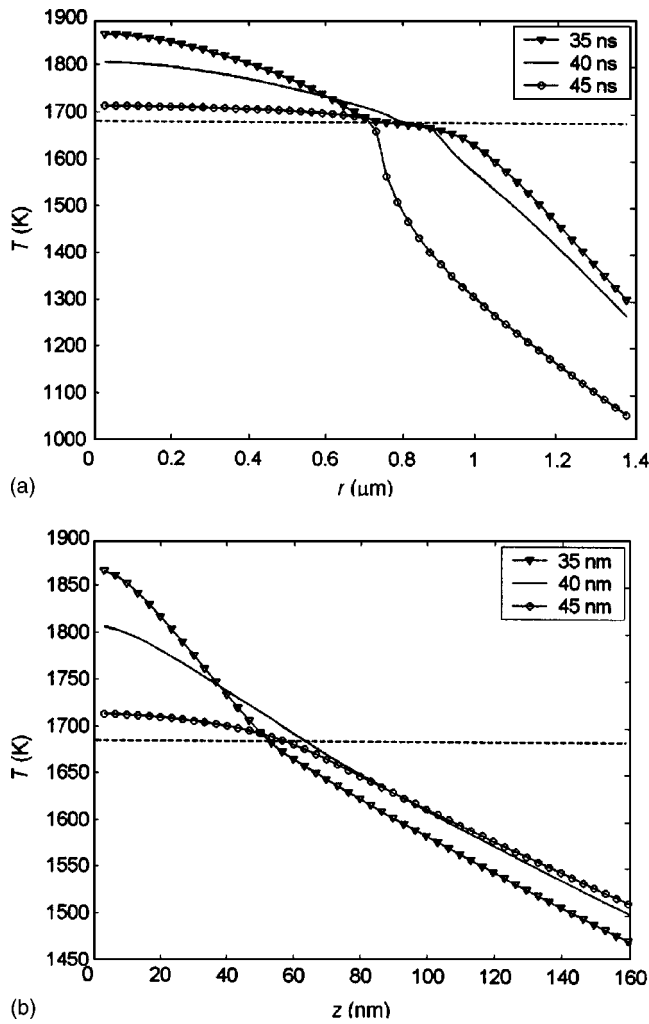


FIG. 4. Temperature distributions: (a) on the surface $T(r, z=0)$ and (b) along the z axis $T(r=0, z)$ for a Gaussian laser pulse at different times around the pulse duration $\tau_l=40$ ns. The dashed horizontal lines indicate $T_{eqm}=1683$ K.

depict the spatial evolution of the interface velocity on the radial (r) and vertical (z) directions of the melted zone. As observed in Fig. 5, v_{sl} and T_{int} from Eq. (8) are almost constant during the solidification stage. From the observed spatial dependence of the interface velocity, we derive the interface temperature field within the material. T_{int} is implemented in the heat and Lambert–Beer equations given by Eqs. (6) and (2), respectively. As shown in Fig. 6, we can therefore compare the transient behaviors of the melt radius and depth, which are obtained from the equilibrium TTFM with $T_{int}=T_{eq,m}$ and out-of-equilibrium TTFM with T_{int} derived from Eq. (8).

The solidification stage is affected by the velocity dependence on T_{int} . As the velocity becomes zero when the maximum radius and depth are reached, the size of the melted zone remains the same in both models. However, in subsequent times, the cooling-stage dynamics is substantially modified when undercooling is considered. The main process parameter affected by the out-of-equilibrium model is the melt lifetime, which is of primary importance for laser processing especially when dopant diffusion is involved during the process.

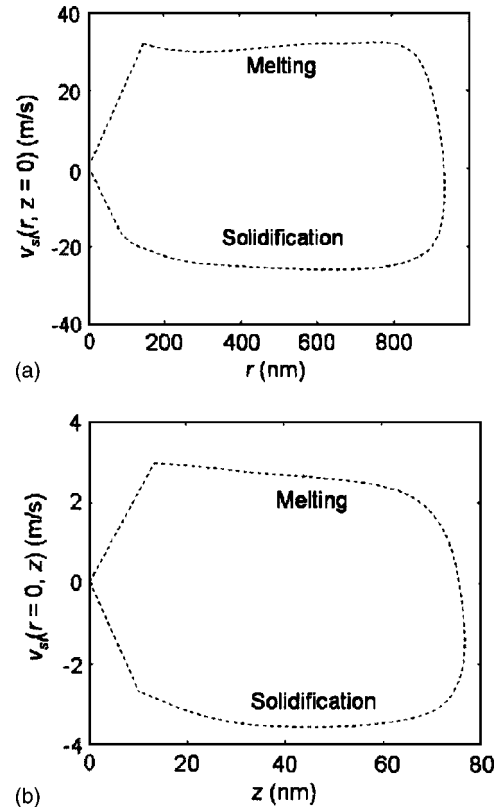


FIG. 5. Interface velocity $v_{sl}(r, z)$ during melting (upper part) and solidification stages (lower part) versus position in the radial (a) and vertical (b) directions.

IV. EXPERIMENTAL RESULTS

To verify our TTFM approach, we perform static and dynamic experimental measurements of the melted surface to obtain the melted zone dimensions, which are successfully compared to the simulation results.

A. Melt-radius measurements

We irradiate a pure Si sample with a frequency-doubled Nd:YAG laser for various intensities and two pulse durations

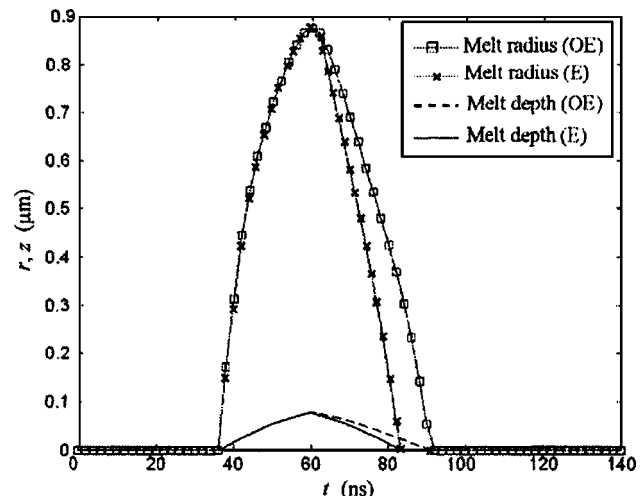


FIG. 6. Melt radius and depth given by the equilibrium (E) and out-of-equilibrium (OE) TTFMs during a 50 ns laser process with a Gaussian beam radius of $1.8 \mu\text{m}$ and fluence of 0.75 J cm^{-2} .

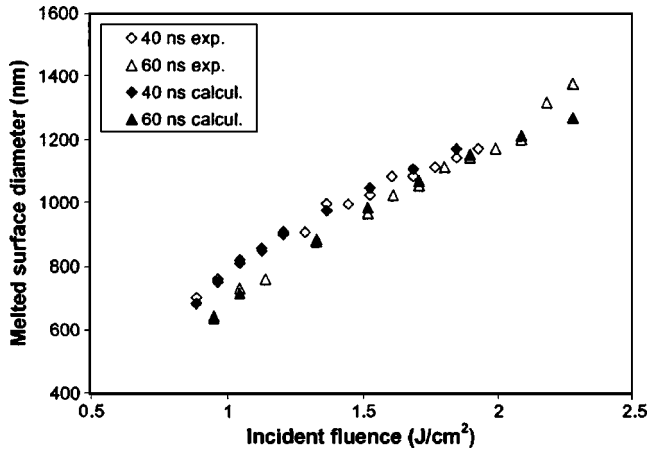


FIG. 7. Melted-surface diameter versus incident-beam fluence: Experimental and calculated results. The Gaussian-beam radius is $0.9 \mu\text{m}$.

of 40 and 60 ns. Since melting induces small surface modifications, we perform AFM measurements of the melted-surface diameter. Experimental data are shown by the open circles and triangles in Fig. 7. The solid points are obtained through both equilibrium and out-of-equilibrium TTFMs owing to a zero interface velocity.

Experimental and computed values of the melted-surface diameter are in excellent agreement, as shown in Fig. 7. We only observe a little discrepancy for a 60 ns pulse and laser fluence higher than 2.1 J cm^{-2} . The relative importance of the surface deformation for those points suggests that this difference could be due to convection effects within the melted zone,¹⁸ which could no longer be neglected at relatively high fluence. Figure 7 clearly shows that, for a given laser fluence, the melted diameter is smaller in the case of long pulse durations. As a consequence, laser fluence is not the only parameter that controls the laser-induced melting process. Moreover, the role played by the incident intensity I appears to be more important than the one played by the pulse duration τ in the resulting laser fluence: $I \times \tau$. This problem was already discussed in Ref. 5.

B. Transient reflectivity measurements

In order to compare the computed transient distribution of the surface temperature with experimental data, we carry out experiments of transient reflectivity measurements. Our technique superposes a continuous-wave HeNe probe laser to the heating Nd:YAG pulsed laser. Since R depends on both T and the phase, the reflected intensity of the HeNe probe laser is a good indicator of the laser-annealing process.¹⁹ However, analysis of the experimental results is not straightforward owing to the phase and temperature dependences of the optical properties. This requires reliable temperature dependencies of the optical reflectivity. Recently, Heller *et al.*²⁰ performed highly accurate measurements of the Si reflectivity at 633 nm in air. The Si surface was oxidized during different times before the measurements, forming SiO_2 layers of 2, 20, and 200 nm. Those authors showed that the SiO_2 layer leads to a clear increase of the temperature depen-

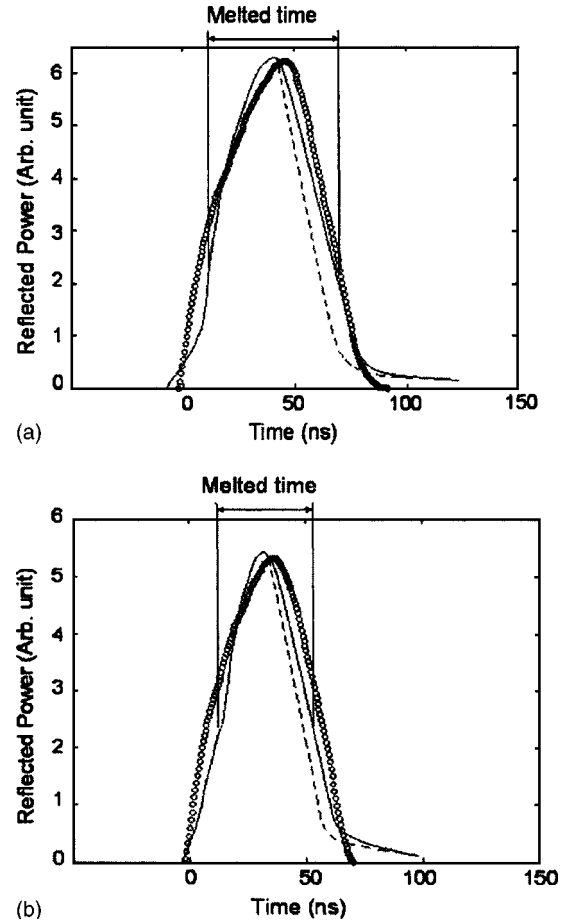


FIG. 8. Transient reflected power measurements of a continuous-wave HeNe laser during a Nd:YAG laser pulse of 50 ns (a) or 40 ns (b). Calculated curves are derived from the equilibrium (dashed line) and out-of-equilibrium (solid line) TTFMs.

dence of R . Due to the presence of such an oxide layer in our experiments, we also take into account this increase of the temperature dependence on R in the TTFM.

The $1/e$ radii of the Nd:YAG and HeNe lasers are evaluated with the knife edge method to $r_{0\text{Nd:YAG}}=0.9 \mu\text{m}$ and $r_{0\text{HeNe}}=3 \mu\text{m}$, respectively. At each laser pulse, we record the time-dependent behavior of the Si-surface reflected intensity from the HeNe probe laser. The choice of a red probing light is driven by the large difference at such a wavelength between the reflectivities of the liquid and solid, which improves the measurement accuracy. The recorded reflected intensities (circles) are given in Fig. 8 for 50 and 40 ns pulse durations. In order to assess the validity of our numerical model, we use the computed surface temperature distribution and achieve the numerical calculation of the transient reflected power during the heating–melting–cooling process using this integral formulation

$$P_{\text{reflected}}(t) = \int_0^{r_{\text{max}}} R(\lambda = 633 \text{ nm}, T(z=0)) e^{-(r/r_{0\text{HeNe}})^2} dr, \quad (9)$$

where $P_{\text{reflected}}$ denotes the dimensionless reflected power. Calculations were performed using both equilibrium (dashed line) and out-of-equilibrium (full line) models. The effect of

the SiO₂ layer on the optical reflectivity of the solid Si at 633 nm is taken into account in the transient reflected power calculation of the probe laser light.

Since the reflected light depends on both surface temperature and melt dimensions, the excellent agreement which is obtained between the experimental and computed curves allows an accurate control of the laser heating, melting, and cooling dynamics. The out-of-equilibrium TTFM, which is only used during the cooling stage of the laser process, clearly improves the quality of the transient reflectivity response. As a consequence, modeling of the undercooling effect is essential for a realistic physical description of a laser-focused annealing process. Moreover, from this experiment, we obtained a proportionality coefficient K of 6.5 cm s⁻¹ K⁻¹ between the interface velocity and temperature in Eq. (8). On the other hand, the comparison between the melt radius and reflected power reveals that the bump in the transient reflectivity evolution lasts longer than the melt duration (i.e., the time during which the melt radius exhibits a steep variation in Fig. 6). Therefore, in the case of a nonuniform laser irradiation, the steep variation of the reflected light intensity is not only caused by the occurrence of molten Si but also by a strong temperature dependence of the solid-Si optical reflectivity.

V. CONCLUSION

Modeling of the transient temperature field and melted-zone dimensions induced from a focused laser process in a bilayer device (such as that shown Fig. 1) with temperature-dependent material parameters was obtained with a new TTFM. Analysis of the melted zone with a high interface velocity enables us to compare the equilibrium and out-of-equilibrium TTFMs. The accuracy of both computed transient temperature field and melted-zone dimensions was validated from experimental measurements. The TTFM is a first and fundamental step for any further modeling of many temperature-driven phenomena, which do not affect the material thermal properties such as impurity diffusion and segregation in laser annealing. As an example, we use the TTFM as the first tool of a software, which performs full bottom up modeling of $n^+-\nu-n^+$ and $p^+-\pi-p^+$ semiconducting resistors^{1,2}

from their fabrication by laser trimming to their electronic operation regime. Such a laser-induced diffusible resistor shows a highly accurate resistance value and is very promising for future analog CMOS technologies. By combining the TTFM with a new out-of-equilibrium diffusion and segregation model, which will be published elsewhere, we are also able to model ultrashallow doping by excimer laser annealing for fabrication of sub-100 nm CMOS devices.

ACKNOWLEDGMENTS

The authors acknowledge the technical help of Jean-Paul L  veque and the financial support of the Natural Science and Engineering Research Council (NSERC) of Canada.

- ¹M. Meunier, Y. Gagnon, Y. Savaria, A. Lacourse, and M. Cadotte, *Appl. Surf. Sci.* **186**, 52 (2002).
- ²M. Meunier, J.-Y. Degorce, J.-N. Gillet, and F. Magny, *Proc. SPIE* **5339**, 265 (2004).
- ³S. C. Chen, C. P. Grigoropoulos, H. K. Park, and P. Kerstens, *J. Appl. Phys.* **85**, 5618 (1999).
- ⁴J.-Y. Degorce, A. Saucier, and M. Meunier, *Appl. Surf. Sci.* **208–209**, 267 (2003).
- ⁵A. Saucier, J.-Y. Degorce, A. Saucier, and M. Meunier, *SIAM (Soc. Ind. Appl. Math.) J. Appl. Math.* **64**, 2076 (2004).
- ⁶R. Cerny, V. Chab, and P. Prikryl, *Comput. Mater. Sci.* **8**, 228 (1997).
- ⁷H. Kisdarjono, A. T. Voustas, and R. Solanki, *J. Appl. Phys.* **94**, 4374 (2003).
- ⁸M. J. Aziz, *Mater. Sci. Eng., A* **226/228**, 255 (1997).
- ⁹N. Chaoui, J. Siegel, J. Solis, and C. N. Alfonso, *J. Appl. Phys.* **89**, 3763 (2001).
- ¹⁰G. E. Jellison, D. H. Lowndes, D. N. Masburn, and R. F. Wood, *Phys. Rev. B* **26**, 2111 (1986).
- ¹¹M. Born and E. Wolf, *Principles of Optics* (Pergamon, Oxford, UK, 1980).
- ¹²D. Bauerle, *Laser Processing and Chemistry* (Springer, Berlin, 2000).
- ¹³S. Whelan, A. La Magna, V. Privitera, G. Mannino, M. Italia, C. Bongiorno, G. Fortunato, and L. Mariucci, *Phys. Rev. B* **67**, 075201 (2003).
- ¹⁴E. M. Sparrow, *J. Heat Transfer* **97**, 333 (1975).
- ¹⁵B. C. Larson, J. Z. Tischler, and D. M. Mills, *J. Mater. Res.* **1**, 144 (1986).
- ¹⁶J. A. Kittl, P. G. Sanders, M. J. Aziz, D. P. Brunco, and M. O. Thompson, *Acta Mater.* **48**, 4797 (2000).
- ¹⁷R. Cerny, R. Sasik, I. Lukes, and V. Chab, *Phys. Rev. B* **44**, 4097 (1991).
- ¹⁸T. Schwartz-Selinger, D. G. Cahill, S.-C. Chen, S.-J. Moon, and C. P. Grigoropoulos, *Phys. Rev. B* **64**, 155323 (2001).
- ¹⁹G. E. Jellison, D. H. Lowndes, D. N. Masburn, and R. F. Wood, *Phys. Rev. B* **34**, 2407 (1986).
- ²⁰J. Heller, J. W. Barthe, C. C. Poon, and C. Tam, *Appl. Phys. Lett.* **75**, 43 (1999).